Radio Science, Volume 30, Number 4, Pages 1065–1083, July–August 1995

The effects of particle size distributions on cross-spectral phase measurements in spatial interferometry

P. B. Chilson,[1] C. W. Ulbrich, and M. F. Larsen,

Department of Physics and Astronomy, Clemson University, Clemson, South Carolina

R. D. Palmer

Department of Electrical Engineering and Center for Electro-Optics, University of Nebraska, Lincoln

S. Fukao, M. Yamamoto, and T. Nakamura

Radio Atmospheric Science Center, Kyoto University, Kyoto, Japan

Abstract. Recent observations made with a 50-MHz Doppler radar interferometer suggest that the presence of precipitation can introduce a bias when using the cross-spectral phase in spatial interferometry that results in an overestimation of the horizontal wind. The process is akin to turbulent fading, which produces a temporal decorrelation in the time history of the complex radar voltages. In the case of precipitation it has been proposed that the size distribution of precipitation particles produces a similar effect. This paper examines the supposition by presenting further data obtained with the 50-MHz Doppler radar. In addition, two simulations, one in the time domain and one in the frequency domain, have been created to test for any biases introduced by an exponential form of the drop size distribution. In the time domain case spectra are generated from simulated time series data, whereas in the frequency domain case the spectra are computed directly. Results from the simulations are given for both the cases of Bragg scatter from turbulent variations in the refractive index and Rayleigh scatter from precipitation particles. This work shows that precipitation does influence the cross-spectral phase data and suggests that spatial interferometry measurements may provide a means of extracting information related to drop size distribution parameters.

1. Introduction

There has been a growing interest in the use of spatial interferometry (SI) in making meteorological observations. The first use of interferometry for the study of atmospheric phenomena came when *Woodman* [1971] used the Jicamarca radar in Peru to measure the inclination of the geomagnetic field lines. Later, *Farley et al.* [1981], also using the Jicamarca radar, were able to refine the techniques used by Woodman by using the cross-spectral information from two receiving antennas to study the strong nighttime plasma turbulence in the equatorial electrojet. In this manner they were able to obtain significantly greater horizontal resolution in their observations compared with other studies conducted at the Jicamarca radar. Radar interferometry observations have been extended lower into the atmosphere by *Röttger et al.* [1990], and *Palmer et al.* [1991], *Van Baelen and Richmond*

[1]Now at Max-Planck-Institut für Aerononie, Katlenburg-Lindau, Germany.

Paper number 95RS00638.
0048-6604/95/95RS-00638$08.00

[1991], and *Larsen et al.* [1992] have shown SI to be a useful tool in measuring the apparent three-dimensional wind vector in the radar scattering volume. We have to make the distinction that the technique estimates the apparent wind, since turbulence leads to a temporal decorrelation of the observed signal, which leads to an overestimation of the horizontal wind. A method to correct for this so-called turbulent fading in the frequency domain has been proposed by *Briggs and Vincent* [1992] and *Sheppard and Larsen* [1992].

Recently the method of spatial interferometry has been applied to the study of yet another atmospheric phenomenon: precipitation. Although the scattering mechanism for precipitation is different from that of turbulent variations in the refractive index, hereafter referred to as "turbulent scatter," the former should be suitable to an SI analysis. That is, a radar signal backscattered from the hydrometeors should provide a means of locating a collection of scatterers within the sampling volume and estimating the three-dimensional velocity vector of the precipitation particles. Measurements reported by *Chilson et al.* [1992] have indeed shown that scatter from precipitation particles does show some of the features characteristic of turbulent scatter. However, the authors reported an overestimation of the horizontal wind when the spatial interferometry formalism was applied. They attributed this to a form of temporal decorrelation resulting from the distribution of the precipitation particle sizes and hence their fall speeds.

We should mention that radar wind estimates in the troposphere are typically made using either of two methods: Doppler beam swinging (DBS) and spaced antenna (SA). A comparison of the two techniques can be found in work by *Van Baelen et al.* [1990]. In the SA method, cross correlations are calculated from backscatter received at two or more spatially separated receiving antennas. The lag times together with the antenna separations are then used in determining the wind velocity [*Röttger and Vincent*, 1978; *Vincent and Röttger*, 1980; *Briggs*, 1984; *Vincent et al.*, 1987; *Larsen and Röttger*, 1989] As mentioned, the newer SI technique can also be used when estimating the wind, and a comparison of SI and SA has been made by *Van Baelen et al.* [1991] and *Sheppard et al.* [1993]. Indeed, the SI technique is the Fourier transform equivalent of the SA technique, that is, analysis in the former is performed in the frequency domain and the latter in the time domain.

In this paper we will develop the idea of using spatial interferometry for the study of precipitation and address the issue of signal decorrelation from particle size distributions. We begin by discussing some of the basic principles of spatial interferometry as applied to the study of scatter from turbulence and precipitation. Then the work of *Chilson et al.* [1992] will be expanded by presenting further examples of data collected at the middle and upper atmosphere(MU) radar during the spring of 1992. Two simulations, one conducted in the time domain and the second in the frequency domain, are then developed to model the amplitude and phase of the cross-spectra resulting from the radar backscatter received in an interferometric mode. In the time domain case spectra are generated from simulated time series data, whereas in the frequency domain case the spectra are computed directly. In particular, the simulations are carried out assuming Bragg scatter from turbulence and Rayleigh scatter from precipitation. Although the two simulation schemes yield similar results, the calculations conducted in the frequency domain are considerably faster. Finally, it will be shown that frequency interferometry measurements of precipitation may provide a means of extracting information related to drop size distribution parameters.

2. Spatial Interferometry

On its most fundamental level the method of spatial interferometry deals with determining the angular position of an ensemble of scattering targets by measuring the phase difference of their backscattered radiation received at two or more spatially separated antennas. With two receiving antennas one can find the projection

of the scattering targets' angular position onto the vertical plane defined by the line connecting the antennas, also called the baseline. To locate the targets in two dimensions, however, a minimum of three antennas is required. Furthermore, by determining the Doppler shift of the received complex signals it is possible to estimate the scatterers' velocity. In spatial interferometry the received signals are comprised of the ensemble average of the signals from all scatterers within the beam. These time series data are Fourier transformed to produce a spectrum in frequency or velocity space. By using the complex voltages from two separate antennas and calculating the cross spectrum, both the amplitude and the phase of the backscattered signal are obtained.

Consider a collection of scatterers advected with a uniform velocity having a horizontal component v_h and a vertical component w. The scatterers are illuminated by a vertically oriented beam and the backscattered radiation is received at two spatially separated antennas i and j having a separation d_{ij}. *Palmer et al.* [1991], *Van Baelen and Richmond* [1991], and *Larsen et al.* [1992] have shown that under these conditions, the phase of the cross spectrum calculated using the two signals can be given by

$$\phi_{ij} = \frac{kd_{ij}}{v_h} \cos(\theta - \theta_{ij})(v_r - w). \qquad (1)$$

In the above equation, k is the radar wavenumber, v_r is the radial velocity, and θ and θ_{ij} are the azimuth angles for the wind vector and the baseline connecting the two antennas, respectively. Solving (1) for two antenna pairs yields the apparent velocity of the scatterers.

An assumption included in the derivation of (1) is that the estimation of w is not affected by aspect sensitivity; that is, the scattering is isotropic within the sampling volume. Any layering of the atmosphere would produce specular backscatter at VHF frequencies [e.g., *Tsuda et al.*, 1986]. Furthermore, if the scattering layer is inclined with respect to the horizontal plane, then the effective radar beam pattern will be shifted from its nominal zenith angle. These conditions result in an erroneous estimation of the vertical wind. *Larsen et al.* [1992] have shown that the effects of aspect sensitivity can also be handled with a spatial interferometry analysis only slightly more complicated than the one presented here. However, *Chu et al.* [1991] found no aspect sensitivity in their observations of radar returns from turbulent variations of the refractive index for a precipitating atmosphere in the region below the 0°C isotherm. Since the primary concern of this work will be to show the variations in the phase of the cross spectra seen in the signal associated with precipitation, the turbulent scatter will be considered isotropic, and no efforts will be made to correct for the effect of specularity in the analysis.

The atmospheric scenario presented above is rather simplistic since antenna illumination pattern effects have not been considered, and all scatterers are assumed to follow constant trajectories in time. Recognizing these limitations, the velocities given in (1) are referred to as the apparent velocities. If a collection of scatterers move uniformly through a radar sampling volume, then a horizontal slice through the volume will contain well-defined bands of constant radial velocity that can be translated into values of zenith angle [*Van Baelen and Richmond*, 1991; *Larsen et al.*, 1992]. Indeed, if the effective antenna illumination pattern were uniform, then there would exist a unique mapping of radial velocity to phase. In reality the antenna pattern is not uniform, and the scatterers near the center of the beam are more intensely illuminated. We should mention here that the presence of aspect-sensitive scattering layers will modify the effective beam pattern of radars operating at VHF, but here we will only be considering isotropic scatter. Since Doppler velocities are sorted into discrete bins, an averaging processes occurs, and a given radial velocity becomes associated with a smaller phase difference [*Van Baelen and Richmond*, 1991]. A further reduction in the cross-spectral phase occurs when the distribution function of the scatterers' ve-

locity becomes nonuniform as in the presence of turbulence. Scatterers at several zenith angles can have the same radial velocity, and an averaging of the values occurs. Stated differently, the temporal decorrelation, or turbulent fading as it is often called, results in a bias in the slope of the cross-spectral phase as a function of radial velocity toward smaller values. This in turn results in an overestimation of the horizontal wind. A frequency domain method has been devised to correct for the turbulent fading and provide the true velocity by *Briggs and Vincent* [1992] and *Sheppard and Larsen* [1992]. The method is called full spectral analysis (FSA) and is the Fourier transform equivalent of the older full correlation analysis (FCA) [e.g., *Meek*, 1980; *Briggs*, 1984], which is performed in the time domain.

3. MU Radar Data

From late April to early May of 1992, a series of experiments were conducted using the MU radar facility located near Shigaraki, Japan (34.85°N, 136.10°E). The primary emphasis of the study was to make wind measurements using different radar techniques at altitudes of roughly 6 to 16 km. During this period a front passed over the island of Japan producing moderate precipitation. On the morning of April 30 the front reached the radar facility producing a 5–8 mm hr^{-1} rainfall rate lasting for about 3 hours. The corresponding radar data were collected while the facility operated in an interferometric mode, as described by *Chilson et al.* [1992].

A pulse width of 1 μs was chosen, which corresponds to a height resolution of 150 m. Furthermore, 64 range bins were sampled beginning at 0.15 km resulting in height coverage from 0.15 to 9.6 km. The operating frequency of the MU radar is 46.5 MHz giving a wavelength of 6.45 m. The interpulse period (IPP) was 400 μs and 256 of the samples were coherently averaged to yield an effective IPP of 0.1024 s and a Nyquist velocity of ± 15.7 m s^{-1}. For the experiment the entire MU radar antenna array was used for transmission giving a 3-dB beamwidth of of 3.6°. For reception, however, three subarrays were used to form the antennas. The array configurations are shown in Figure 1.

To apply the methods of spatial interferometry to the observations of the precipitation, we must first find the auto- and cross spectra for the given antenna combinations. Spectra were calculated for the precipitation data using 128 time series points with each spectrum corresponding to 10 incoherent integrations. An example of the resulting cross spectra can be seen in Figure 2, where negative velocities indicate motion towards the radar. Furthermore, the spectra have been plotted using a linear power spectral density scale and have been normalized to the largest autospectral peak at each altitude. The Figure contains the cross spectra calculated from the baseline pairs 1–2, 1–3, and 2–3 shown in Figure 1. It should be noted that the recovery time of the transmit/receive switch produced excessive noise in all gates below approximately 1.8 km. Also note that some spectra contain two peaks, representing contributions from both the hydrometeors and the turbulent variations of the refractive index.

The interesting feature in Figure 2 is the separate linear trends in both the cross-spectral phase corresponding to Bragg scatter from the

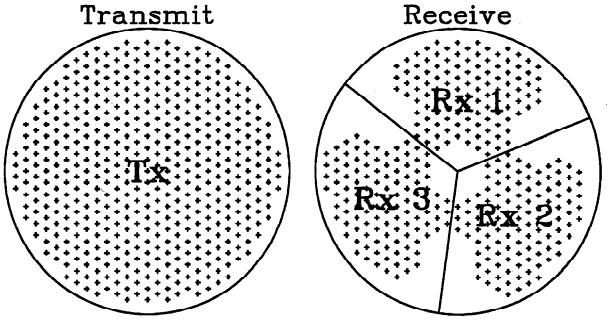

Baseline	Angle	Distance
1 – 2	157.58°	52.52 m
1 – 3	217.58°	52.52 m
2 – 3	277.58°	52.52 m

Figure 1. Diagram showing the configuration of the MU antenna array used in the experiment.

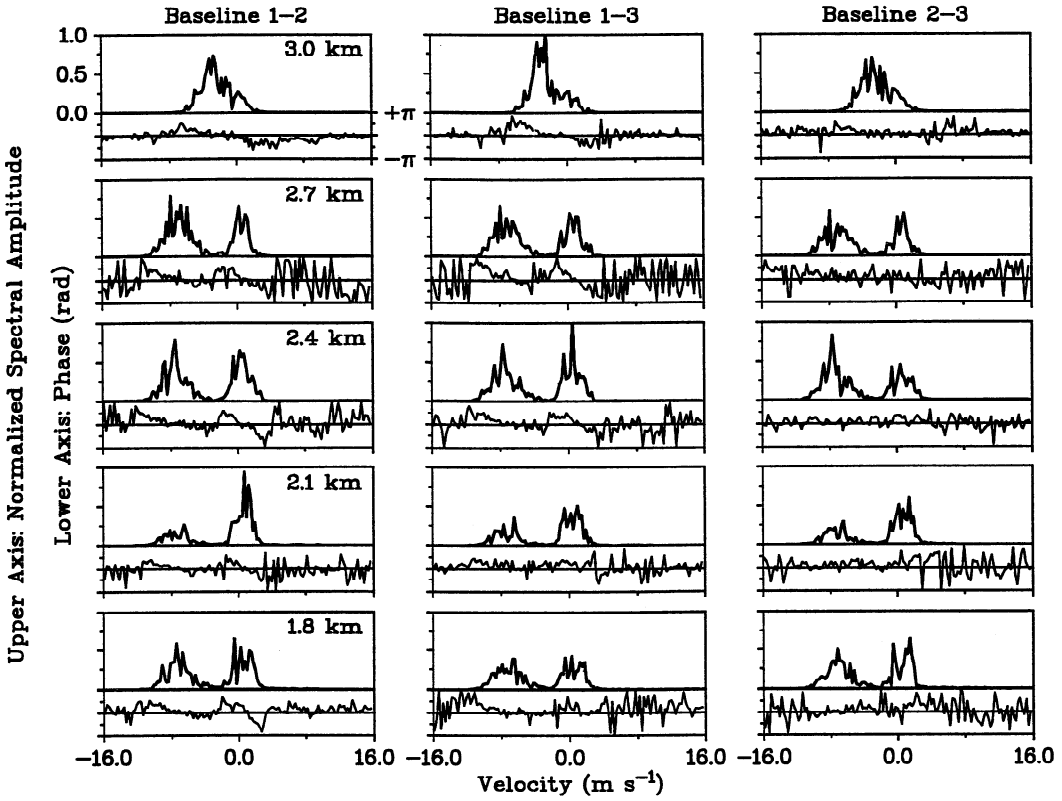

Figure 2. Cross spectra for heights ranging from 1.8 to 3.0 km plotted for the three antenna pairs shown in Figure 1. The cross spectra have all been normalized to the autospectrum of the corresponding height.

turbulence (right-most peaks) and Rayleigh scatter from the precipitation (left-most peaks). For a given spectral peak, the cross-spectral amplitude relative to the autospectral amplitude is a measure of the coherence. Therefore, only regions of the cross spectrum where the relative amplitudes are large should exhibit consistency in the phase. Also, as seen in (1), the slope of the cross-spectral phase as a function of radial velocity is greatest when the horizontal wind vector is parallel to one of the antenna baselines. This situation represents a condition of minimal spatial decorrelation. Estimates of the apparent wind have been made using the phase corresponding to the turbulent peak for the range of heights shown in Figure 2. The results show the wind to be mostly southerly at altitudes of 2.1 to 2.7 km. At 1.8 km the wind was south-southeast, and at 3.0 km it was south-southwest. Since the 2–3 baseline is almost perpendicular to a southerly wind, the cross-spectral phase for that baseline shows a small slope in Figure 2 for altitudes between 2.1 and 3.0 km.

Since no correction has been made in Figure 2 for the effects of turbulent fading, the slopes might be underestimated; that is, the corresponding horizontal wind magnitude will be overestimated. Furthermore, we see that the slopes of the phase from the precipitation return have still smaller values than those obtained from the turbulence signals. The slope is a measure of the apparent horizontal winds, and the quotient of slope and intercept for the fitted line is a measure of the vertical wind if there are no aspect sensitivity effects [*Larsen et al.*, 1992; *Sheppard et al.*, 1993]. The observed Doppler velocities in the precipitation portion of the spectrum represent not only the particle fall speeds

but turbulent broadening and beam broadening as well. Under the assumption that a collection of hydrometeors having the same size is carried along by a horizontal wind, the slopes in the cross-spectral phase associated with the turbulent peak and the precipitation peak should be approximately the same. The primary difference in the two would be in the intercepts, which are affected by the magnitude of the radial velocity. The data in Figure 2 clearly show this not to be the case. The phase slopes associated with the turbulence are more steeply inclined than those associated with the precipitation. Although reduction in the cross-spectral phase slope is typically associated with turbulent fading, it was proposed by *Chilson et al.* [1992] that scatter from a collection of precipitation particles having a range of sizes can lead to similar results. That is, the broadening of the spectrum due to the distribution of particle fall speeds has a similar effect on the cross-spectral slope as the broadening from turbulence.

4. Time-Domain Simulation

To study the possible effects of a distribution of precipitation particle sizes on the cross-spectral phase, we have developed a simple simulation patterned after the results reported in the last section. The calculations are not meant to be a rigorous treatment of atmospheric scattering mechanisms but rather should illustrate how precipitation particles can bias the cross-spectral phases. The time series data for precipitation and air motions were generated for a given velocity distribution of the scatterers, an antenna radiation field pattern, a radar wavelength, and the antenna orientations. Cross spectra were then calculated using the simulated time series results. The calculation assumes that the scattered power from the turbulent variations of the refractive index results from a collection of discrete parcels of air, and the parcels are assumed to be isotropic scatterers having random reflectivity. In addition, the velocity distributions of these parcels are approximated by Gaussian functions in three dimensions. The power resulting from the precipitation scatterers is assumed to be similarly distributed in velocity; that is, they are coupled to the atmospheric medium, but with an additional parameter associated with the particles' terminal fall speeds. For calculations of the scattered power the Rayleigh approximation will be used.

The method of calculation is similar to a model presented by *Sheppard and Larsen* [1992] that they used to show the equivalence of SA and SI radar measurements. Whereas the work of Sheppard and Larsen only considered the echo signals from clear-air turbulence, the current treatment accounts for both Bragg scatter from turbulence and Rayleigh scatter from precipitation. To generate the time series data, a large number of scatterers are randomly located in a volume of space and then allowed to move according to certain governing equations, that is, the velocity distributions. Each target is assigned a backscattering cross section, and the time series data are calculated by summing the contributions from all the scatterers within the radar sampling volume. A separate time series data point is generated for three separate receiving antennas.

We begin by considering the case of turbulent motions of discrete parcels of air. Initially the parcels are randomly distributed in a volume of Cartesian space V_{init}, with the radar sampling volume being a subset of that space. Although the parcels are free to move, the dimensions of the space V_{init} are chosen such that the radar beam will always contain scattering targets as the simulation progresses in time. As an example, assume the parcels to be traveling with a mean vertical velocity w_o, and the dwell time for calculating one spectrum is t_d. The vertical extent of V_{init} would have to be $w_o t_d$ larger than the height of the radar sampling volume to allow new targets to enter into the beam. See for example Figure 1 of *Sheppard and Larsen* [1992].

The radar sampling volume is calculated from assumed values of the pulse width and the radar beam width. Although many choose to use a Gaussian distribution when approximating the

magnitude of the radar's radiation field, this approximation has limitations. The intensity of the beam only reaches a null for a zenith angle $\delta = \pm\pi/2$. For the present simulation and the one presented in the following section, the radiation field amplitude will be described by a sinc function as given by

$$U(\delta) = \frac{\sin \kappa_{bw}\delta}{\kappa_{bw}\delta}. \quad (2)$$

The coefficient κ_{bw} is a width scaling factor and is equal to $2.780/\delta_{bw}$, with δ_{bw} being the 3-dB beamwidth in radians. The time domain simulation also assumes a triangular pulse weighting function $\tau(r)$.

A complex time series voltage can be found for a given receiving antenna by vectorially summing the amplitude and phase of all scatterers contained in the sampling volume. Only scatterers located between the first nulls of the beam are used in the summation. If the jth parcel of air is in the pulse volume, then it is assigned a backscattered field amplitude A_j, which is a uniform random variate bounded by $A_{\min}$ and $A_{\max}$. Certainly this does not realistically model the scattering mechanisms present in the atmosphere. It should, however, provide an approximation to the complex radar time histories resulting from motions of the atmosphere. The backscattered field amplitude is additionally weighted by $\tau_j = \tau(r_j)$ and $U_j = U(\delta_j)$, where the range and zenith angle of the jth parcel of air are given by r_j and δ_j, respectively. The phase is then found through the equation $\varphi = k(r_j + r_{jk})$, where k is the radar wavenumber, and r_{jk} is the distance of the jth parcel from the kth antenna.

After each summation the scatterers are assigned new spatial coordinates as prescribed by their velocity distributions. That is, a scatterer j at location $\vec{r}_j$ is assigned a wind vector $\vec{v}_j$, and its new position becomes $\vec{r}_j{}' = \vec{r}_j + \vec{v}_j\, t_s$, where t_s is the sampling period. The wind vector is defined by the components u_j, v_j, and w_j. Each component is assumed to be an independent random variate having a distribution function approximated by a Gaussian function [*Woodman and Guillén*, 1974],

$$f_\eta(\eta) = (2\pi\sigma_\eta^2)^{-1/2} \exp\left[-\frac{(\eta - \eta_o)^2}{2\sigma_\eta^2}\right], \quad (3)$$

where η is replaced by u, v, or w. The variance is given by σ_η^2, and η_o is the mean velocity. The process is repeated a number of times to construct the time history of complex voltages. The time series data are then used in the calculation of the spectra and correlations.

To simulate scatter from rain, a collection of precipitation particles is also randomly distributed in space during the initial sampling pulse, but in addition, the particles are assigned individual diameters. The particles' diameters are read in from a file created using a form of the drop size distribution (DSD) given by [*Ulbrich*, 1983]

$$N(D) = N_o D^\mu e^{-\Lambda D}, \quad (4)$$

where $N(D)$ is the number of precipitation particles of diameter D per unit diameter interval, and N_o, Λ, and μ are parameters of the distribution. As will be shown later, *Marshall and Palmer* [1948] showed a dependence between the value of Λ and the rainfall rate. In addition, *Ulbrich* [1983] has proposed an exponential relationship between the values of N_o and μ. For the present simulation μ will be set equal to zero.

An exponential DSD favors smaller particle diameters, and although $5\text{x}10^5$ scatterers were used in the simulation, the larger particles tended to be under-represented. Therefore, the fall speeds of the precipitation particles showed a bias towards smaller values. Once assigned, the particles maintain the same diameters in the simulation for all subsequent sample pulses. Admittedly, there are many processes that lead to particle growth and breakup, but they are not being considered here. On the average, the diameters remain the same provided N_o and Λ do not change.

The process of simulating the time series data for precipitation is similar to that of turbu-

lence. The difference lies in the calculation of A_j and $\vec{v}_j$. Since precipitation particles in the Rayleigh approximation act as electric dipoles, the backscattered field amplitude A_j should be proportional to the particle diameter cubed. The fall speeds of the precipitation particles are also related to the diameters. The simulation assumes the fall speed to be given by $w_f = aD^b$, where D is the diameter. A listing of various values of a and b as well as the role of the power law form of the fall speed relation in calculations of rainfall parameters from Doppler spectra can be found in *Atlas et al.* [1973]. The velocities of the precipitation particles are also affected by the motions of the air through which they are falling. Therefore the velocity vector of the jth precipitation particle is given by $\vec{v}_j = (u_j, v_j, w_j + w_{fj})$. In reality the motions of the wind and precipitation are coupled through the frictional drag of the particles. The effects should be small for the environmental conditions being simulated and will not be considered.

The simulation has been run assuming three receiving antennas placed at the vertices of an equilateral triangle. The baseline separation of the antennas was chosen to be 50 m to replicate the MU radar antenna configuration. A diagram showing the antenna arrangement used in the simulation is given in Figure 3. Input data that were allowed to vary between the different runs of the simulation included the parameters describing the motions of the atmosphere and the distribution of the precipitation particles. Additional parameters used in the calculations involved those connected with the experiment itself and were held constant. These included the antenna illumination pattern, antenna locations, radar wavelength, and the radar sampling period. The radar sampling period was used to calculate the Nyquist velocity. A list of these quantities is given in Table 1. The values for a and b shown in the Table were taken from *Spilhaus* [1948].

To consider the effects of turbulence and precipitation on the cross-spectral phase, we will consider the results from different runs of the

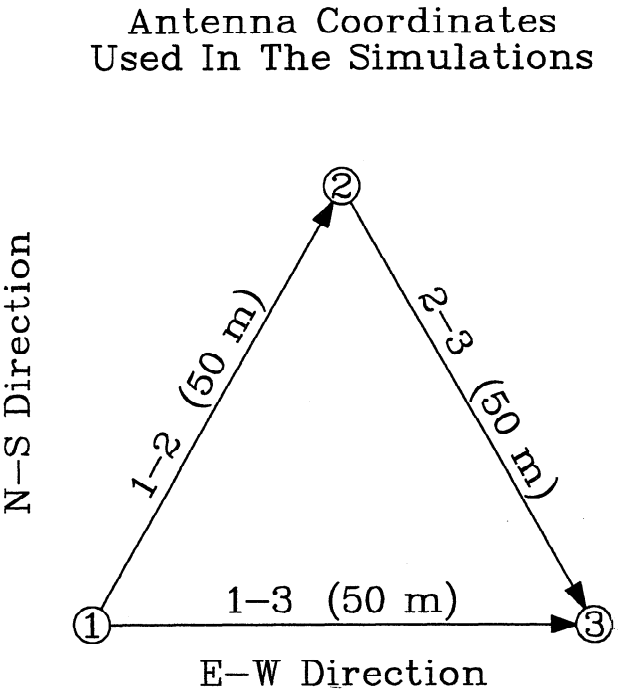

Figure 3. The locations and separation distances of the three antennas used in the time and frequency domain simulations.

simulation program: some including turbulence, and the others including turbulence and precipitation. In all the cases a zonal wind having a magnitude of 40 m s^{-1} was assumed, and the meridional and vertical components were set equal to zero. Turbulence was included by assigning nonzero values to the variances of the wind vector components, $\sigma_u^2 = \sigma_v^2 = 9$ m^2 s^{-2} and $\sigma_w^2 = 0.5$ m^2 s^{-2}. Large values were chosen for σ_u^2 and σ_v^2 since the slope of the cross-spectral phase is rather insensitive to fluctuations in the horizontal plane for a vertically oriented beam. Although not representative of stratiform rain conditions, these values are not unrealistic [*Doviak and Zrnić* 1984], and have been chosen to test the simulation under extreme conditions. To account for scatter from precipitation, two files were created containing the collections of hydrometeors used in the analysis. The first file was generated using a value of Λ in (4) of 20 cm^{-1} and the second using $\Lambda = 40$ cm^{-1}. The two cases will be considered separately.

Table 1. Constant Input Parameters for the Simulations

Parameter	Symbol	Value
Radar wavelength	λ	6.5 m
Antenna separation	d_{ij}	50.0 m
Half-power beam width	θ_{bw}	3.6°
Sampling time	t_s	0.1 s
Power law coefficient	a	14.2 m s^{-1} cm^{-b}
Power law coefficient	b	0.5

The simulated cross spectra are presented in Figure 4, where the results correspond to measurements made along the 1–3 baseline, that is, parallel to the wind vector. The upper panel shows the cross spectrum generated for the case of air motion and no precipitation. Each cross spectrum has been normalized to the peak of its corresponding autospectrum. When there is no decorrelation, the slope of the cross-spectral phase should be approximately equal to kd/v_h as shown in (1). In the panels of Figure 4 a dashed line has been included to indicate the expected slope and intercept of the cross-spectral phase assuming zero turbulent fading effects. Note that the turbulence included in the simulation was not sufficient to appreciably bias the slope of the cross-spectral phase shown in the upper panel. The lower two panels show the cross spectra that have been produced by assuming scatter from precipitation particles having DSDs with Λ given by 40 and 20 cm^{-1}. Although the precipitation particles are affected by the air motions, the plots in the lower panel contain no backscatter from the turbulent scatterers.

The case where $\Lambda = 40$ cm^{-1} represents a conservative test of the DSD's effects on the cross-spectral phase. Using the expression relating Λ to the rainfall rate (millimeters per hour) reported by *Marshall and Palmer* [1948], $\Lambda = 41R^{-0.21}$, we find that a Λ value of 40 cm^{-1} corresponds to a rainfall rate of only 1.1 mm hr^{-1}. Although the cross-spectral

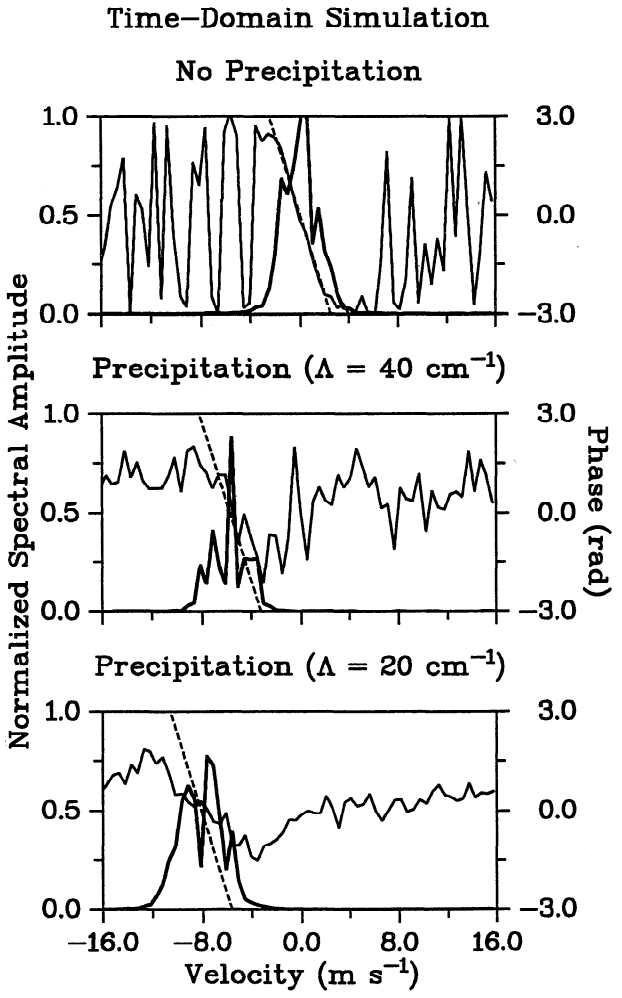

Figure 4. Cross-spectra calculated in the time domain resulting from parcels of air (upper panel) and precipitation particles (lower panels) being advected by a horizontal wind through a turbulent medium. The plots correspond to the 1–3 baseline. Dashed lines have been included to indicate the expected slope and intercept of the cross-spectral phase assuming zero turbulent fading effects. The input parameters were $u = 40$ m s^{-1}, $v = w = 0$, $\sigma_u^2 = \sigma_v^2 = 9$ m^2 s^{-2}, and $\sigma_w^2 = 0.25$ m^2 s^{-2}.

phase is rather jagged, the slope has been slightly biased by the presence of the precipitation particles. Here the dashed line has been shifted horizontally by an amount consistent with the expected mean Doppler fall speed of the precipitation particles. The jagged appearance in the cross-spectral amplitude and phase results from the effects of decorrelation, and the spectra would become smoother with more incoherent integrations. The spectra shown in Figure 4 represent only five coherent integrations as an attempt to better replicate the MU radar observations.

In the lower panel of Figure 4 a heavier rainfall has been simulated by assuming a value of Λ equal to 20 cm^{-1}. Using this value of Λ in the *Marshall and Palmer* [1948] expression gives a rainfall rate $R = 30$ mm hr^{-1}. This time the slope of the cross-spectral phase is clearly biased towards zero. Recall that temporal decorrelations are produced in the complex radar time histories if the velocity vectors associated with a collection of scatterers are allowed to deviate from their mean value. Although the deviations are usually associated with turbulence, the distribution of precipitation fall speeds would also produce such deviations in the radial velocity. Since a smaller value of Λ in the DSD corresponds to a broader distribution of fall speeds, we should expect a greater degree of fading. Figure 4 indeed demonstrates this trend and supports the argument that differences in cross-spectral phase slopes found in the MU radar data are caused by temporal decorrelations that result from the size distribution of the hydrometeors. The "precipitation fading" mechanism is similar to that of turbulent fading.

5. Frequency Domain Simulation

The results of the last section indicate that the SI method may provide a means of extracting precipitation parameters from the observed cross spectra. The calculations, however, are too time consuming to be used in an iterative simulation process for determining the dependence of the cross-spectral phase on the form of the drop size distribution. Therefore a second simulation is now presented that requires less calculation time. These calculations are performed entirely in the velocity, that is, frequency domain by constructing spectra using only the velocity distributions of a collection of atmospheric targets, their scattering cross sections, and the radar beam pattern. As in the last section, echo signals from turbulent variations in the refractive index are treated by considering discrete parcels of air as scattering targets having velocity distributions described by Gaussian functions. From these Gaussian functions a resulting distribution given by the sum of the horizontal and vertical components can be calculated. The velocity distribution of the precipitation particles is found through the drop size distribution and an equation relating the particles' diameters to their fall speeds. The cross spectrum is then calculated for a given pair of receiving antennas with known locations.

First consider the case of scatter from the turbulent variations in the refractive index or turbulent scatter. As in the time domain simulation, the wind vector is described by three independent Gaussian distributions for the u, v, and w components. The quantity in which we are really interested is the distribution of the radial velocities. The radial velocity for a scatterer is found by calculating the scalar product of the velocity vector and the unit vector locating the scatterer. The result is

$$v_r = u \sin\theta \sin\delta + v \cos\theta \sin\delta + w \cos\delta, \quad (5)$$

where θ and δ are the azimuth and zenith angles, respectively. Using this equation along with the Gaussian distribution function for the u, v, and w components, we can find a distribution function for the radial velocities.

To begin a treatment of the problem, first consider a random variable $\mathbf{x}$ that takes the values x, such that the distribution of all possible values is given by $f_x(x)$. If a second random variable $\mathbf{y}$ is linearly related to $\mathbf{x}$ through the equation $\mathbf{y} = a\mathbf{x} + b$, where a and b are constants,

then the distribution function of $\mathbf{y}$ is given by [*Papoulis*, 1991]

$$f_y(y) = \frac{1}{|a|} f_x\left(\frac{y-b}{a}\right). \quad (6)$$

Next consider two independent random variables $\mathbf{x}$ and $\mathbf{y}$ having distribution functions $f_x(x)$ and $f_y(y)$, respectively. The distribution function of $\mathbf{z} = \mathbf{x} + \mathbf{y}$ is found through the convolution integral [*Papoulis*, 1991]

$$f_z(z) = \int_{-\infty}^{\infty} f_x(z-y) f_y(y) dy. \quad (7)$$

The analysis is easily extended to include a summation of three independent random variates. To find the distribution function of radial velocities, (3) is used in conjunction with (6) and (7) to produce

$$f_{v_r}(v_r) = \frac{1}{|\sin\theta \sin\delta|} \cdot I, \quad (8)$$

where

$$I = \int_{-\infty}^{\infty}\int_{-\infty}^{\infty} f_u[a(v,w)] f_v(v) f_w(w) dv dw \quad (9)$$

and

$$a(v,w) = \left(\frac{v_r - v\cos\theta\sin\delta - w\cos\delta}{\sin\theta\sin\delta}\right). \quad (10)$$

Assuming that the atmospheric parameters remain constant, the solution to the integral is actually a function of the radial velocity, the azimuth angle, and the zenith angle. The solution to the convolution integral is given by

$$f_{v_r}(v_r,\theta,\delta) = (2\pi\sigma_r^2)^{-1/2} \exp\left[-\frac{(v_r - v_{ro})^2)}{2\sigma_r^2}\right], \quad (11)$$

where

$$v_{ro} = u_o \sin\theta\sin\delta + v_o\cos\theta\sin\delta + w_o\cos\delta \quad (12)$$

and

$$\sigma_r^2 = \sigma_u^2\sin^2\theta\sin^2\delta + \sigma_v^2\cos^2\theta\sin^2\delta + \sigma_w^2\cos^2\delta. \quad (13)$$

The solution gives the distribution of all possible radial velocities oriented along a particular line of sight direction described by θ and δ.

The distribution given above can be simplified by making an assumption concerning the nature of the turbulence. First note that the azimuthal terms in (12) can be removed since $u_o\sin\theta + v_o\cos\theta$ is just the mean horizontal velocity of the scatterers v_{ho}, which is equivalent to $(u_o^2+v_o^2)^{1/2}$. We can also remove the θ dependence from (13) by assuming the magnitude of the zonal turbulence to be approximately equal to the meridional turbulence. Then the horizontal contribution to the radial variance σ_r^2 simply becomes $\sigma_h^2\sin^2\delta$, where the horizontal variance is $\sigma_h^2 \approx \sigma_u^2 + \sigma_v^2$. This assumption will be used in the subsequent analysis.

To find the distribution of radial velocities for the case of precipitation first recall the form of the DSD shown in (4). Given a relation between the precipitation particles' diameters and their fall speeds, we can transform the DSD into a distribution in velocity. Using the power law equation $w_f = aD^b$, the distribution of precipitation fall speeds can be expressed as

$$g_{w_f}(w_f) = \frac{N_o}{ab}\exp\left[-\Lambda\left(\frac{w_f}{a}\right)^{1/b}\right]\left(\frac{w_f}{a}\right)^{\frac{1+\mu-b}{b}}. \quad (14)$$

The above equation is only valid in the absence of turbulence or wind. If the motion of the air is considered, and the precipitation particles are advected with the wind, then the radial velocity of the hydrometeors is given by

$$v_r = v_h\sin\delta + w\cos\delta + w_f\cos\delta, \quad (15)$$

where v_h is the horizontal velocity. Note that the azimuthal dependence in (15) has been absorbed in the v_h term. The radial velocity solution for the distribution function is then obtained through the convolution of (8) – (10) and (14),

$$g_{v_r}(v_r,\delta) = \frac{1}{|\cos\delta|}\int_{-\infty}^{\infty} f_{v_r}(v_r - w_f,\delta) \cdot g_{w_f}(w_f) dw_f. \quad (16)$$

By invoking the convolution integral, we have assumed that the quiescent fall speeds of hydrometeors, that is, the fall speed through still air, and the motions of the air particles are independent. As in the last section, we will be ignoring the frictional drag of the precipitation particles. A simple closed form solution to (16) does not exist, and the integral must be solved numerically.

Next we calculate the spectrum that would be observed assuming an extremely thin radar beam oriented along a particular line of sight direction. The spectrum can be calculated by finding the distribution of radial velocities for that orientation and associating a weighting factor with each velocity term representing its total backscattered power. The resulting power-weighted distribution (PWD) will be denoted by $\beta_{v_r}(v_r, \delta)$. The PWD is proportional to the spectrum that would result from a thin radar beam. When dealing with turbulent scatter, if we assume that each parcel of air has the same backscattering cross section and is therefore independent of velocity, then the PWD is simply equal to the distribution function calculated earlier, or

$$\beta_{tv_r}(v_r, \delta) = f_{v_r}(v_r, \delta). \tag{17}$$

Actually, there are mechanisms coupling the magnitude of the wind and the level of turbulence. For example, *Sidi and Barat* [1986] have observed thin layers in the stratosphere occurring at regular intervals in height. The transition between the layers is characterized by variations in the wind and pockets of clear-air turbulence. This feature was not reported in the troposphere. For precipitation, backscattering power is proportional to the sixth power of the particles' diameters and is therefore related to the fall speed. Incorporating the power law relation $w_f = aD^b$ into (16), we find the PWD for precipitation to be

$$\beta_{pv_r}(v_r, \delta) = \frac{1}{|\cos\delta|} \int_{-\infty}^{\infty} f_{v_r}(v_r - w_f, \delta) \cdot g_{w_f}(w_f) \left(\frac{w_f}{a}\right)^{6/b} dw_f. \tag{18}$$

To calculate the final Doppler spectrum, we must find the summation of all PWDs weighted by the radar field intensity for a given line of sight direction. It will be assumed that the beam width of the transmitted beam does not differ significantly from that of the receiving beam. When this is not the case, then it will be necessary to model the two beams separately. An illustration of the calculation is shown in Figure 5. The peaks in the Figure represent the PWDs that would be found assuming scatter from parcels of air being advected with a horizontal wind and no vertical wind through a turbulent medium. Furthermore, for the sake of illustration it has been assumed that the vertical component of the turbulence is zero. The total power associated with each peak has been weighted by the beam pattern. The Doppler spectrum is then formed by summing contributions from all of the peaks. The cross spectrum is similarly calculated with the inclusion of a term to account for the phase difference. Representing the summation as an integral, the cross spectrum calculated from antennas i and j is given by the equation

$$S_{ij}(v_r) = \int_{-\pi/2}^{\pi/2} \beta_{v_r}(v_r, \delta) U^2(\delta) \cdot \exp[ikd_{ij}\cos(\theta - \theta_{ij})\sin\delta] d\delta, \tag{19}$$

where d_{ij} is the separation of the two antennas, θ_{ij} is the azimuth angle of their baseline, and θ is the azimuth angle of the wind. The PWD β_{vr} is used to denote either β_{tv_r} for the case of turbulence or β_{pv_r} for precipitation. The radiation field amplitude is given by $U(\delta)$.

A program has been written that incorporates the ideas outlined above to calculate the cross spectrum for various atmospheric conditions. As seen from (11) and (17) for turbulence, the power-weighted distribution function can be calculated given the mean and variance of the u, v, and w components of the wind. A similar calculation for precipitation, that is, using (16) and (18), requires the additional parameters of the DSD and those used in the equation

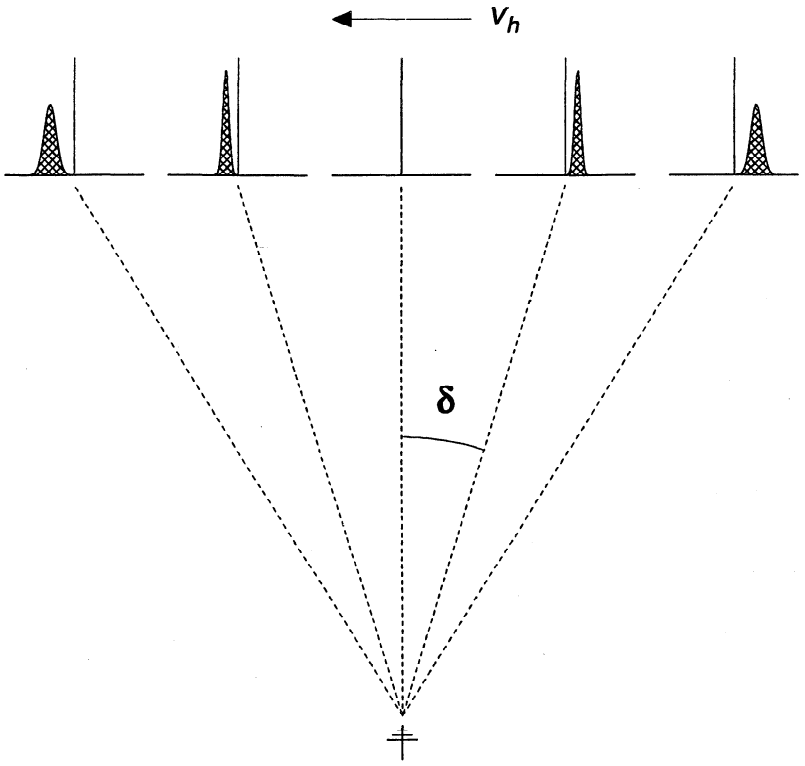

Figure 5. Illustration of how the Doppler spectrum is calculated in the frequency domain simulation by summing different spectral contributions for different zenith angles.

$w_f = aD^b$. The coefficients in the power law relation will be held fixed for the present but will be allowed to assume different values in the following section. Again a sinc function has been assumed for the antenna radiation field amplitude as given in (2). In calculating the integral given in (19) a smaller range of zenith angles was used, with the range divided into 200 increments. The limits of the integral were given by the location of the fifth null in the sinc function. A listing of the constant input parameters for the simulation is given in Table 1.

Cross spectra have been generated from the frequency domain simulation using the same atmospheric input parameters as used to produce the plots shown in Figure 4. Likewise, the same antenna geometry and all of the constant input parameters given Table 1 were used. These results are presented in Figure 6, where again the upper panel shows the turbulent peak and the lower panels show the precipitation peaks. Note that the cross spectra are similar to those calculated in the time domain simulation. Since the cross spectrum is produced independently of the autospectrum, the former has been normalized to one.

As in the last section, a dashed line has been included in the plots to show the cross-spectral phase for a condition of zero decorrelation. Looking at the cross-spectral phases in Figure 6, we notice that the frequency domain simulation has also predicted a noticeable bias in the slopes for the two cases of $\Lambda = 40$ cm^{-1} and $\Lambda = 20$ cm^{-1}. Here again μ has been set equal to zero in the DSD. The biases predicted by the time domain simulation seem to show a lesser reduction in slope than that given by the frequency domain simulation. However, in both simulations the smaller value of Λ is found to produce the larger decorrelation. This trend again supports

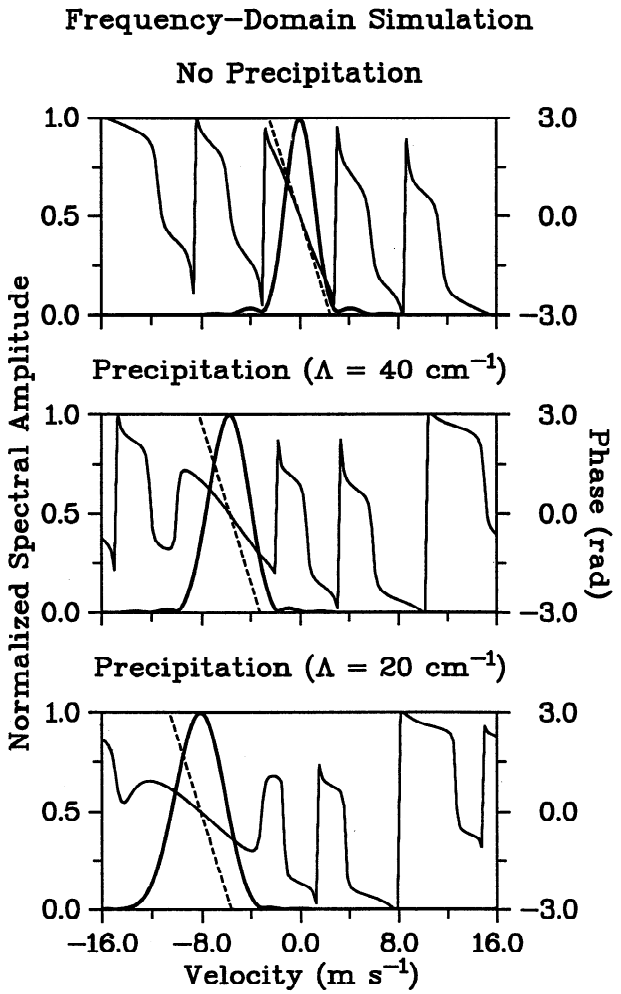

Figure 6. Cross spectra calculated in the frequency domain resulting from parcels of air (upper panel) and precipitation particles (lower panels) being advected by a horizontal wind through a turbulent medium. The plots correspond to the 1–3 baseline. Dashed lines have been included to indicate the expected slope and intercept of the cross-spectral phase assuming zero turbulent fading effects. The input parameters are the same as given in Figure 4.

the argument that heavier rainfall rates produce greater decorrelation leading to a reduction in the slope of the cross-spectral phase.

6. Comparisons of the Results

The advantage of calculating the cross spectra in the frequency domain as opposed to the time domain lies in the relative speeds of the two methods. The computer on which the simulations were run required several hours to calculate one of the cross spectra in the time domain from the parameters given in Table 1. The calculations carried out in the frequency domain using the same input parameters required less than a minute.

Given the speed with which the predictions can be made in the frequency domain, cross spectra were generated for a range of Λ values assuming different values for the wind. In addition, two sets of parameters for the relation $w_f = aD^b$ were assumed. The first set is that of *Spilhaus* [1948]: $a = 14.2$ and $b = 0.5$. The second set, which has been taken from *Sekhon and Srivastava* [1971], corresponds to data obtained during a thunderstorm: $a = 16.9$ and $b = 0.6$. The value of a has the units m s^{-1} cm^{-b}. *Atlas and Ulbrich* [1977] found that the values of $a = 17.67$ and $b = 0.67$ gave good results for a number of precipitation observations. These values are not far different from those of *Sekhon and Srivastava* [1971]. For comparison, the time domain simulation has also been run using the same fall speed law parameters as for the frequency domain simulation but using only two of the values of Λ.

The results of the calculations have been used to find the ratio of the slopes in the cross-spectral phase corresponding to air motion and precipitation. These ratios have been plotted in Figure 7 as a function of Λ for six different combinations of u, v, w, σ_u, σ_v, and σ_w. In each case the cross spectra were produced assuming the antenna pair to be parallel to the horizontal wind vector. As is true for the spectra shown in Figure 4, the points plotted in Figure 7 for the time domain simulations were calculated using only five coherent integrations. The slope of the cross-spectral phase is inversely proportional to the apparent horizontal wind velocity that would be estimated using SI. Consequently, the ratio of the turbulent slope and the precipitation slope indicates by what factor the apparent horizontal wind would be overestimated

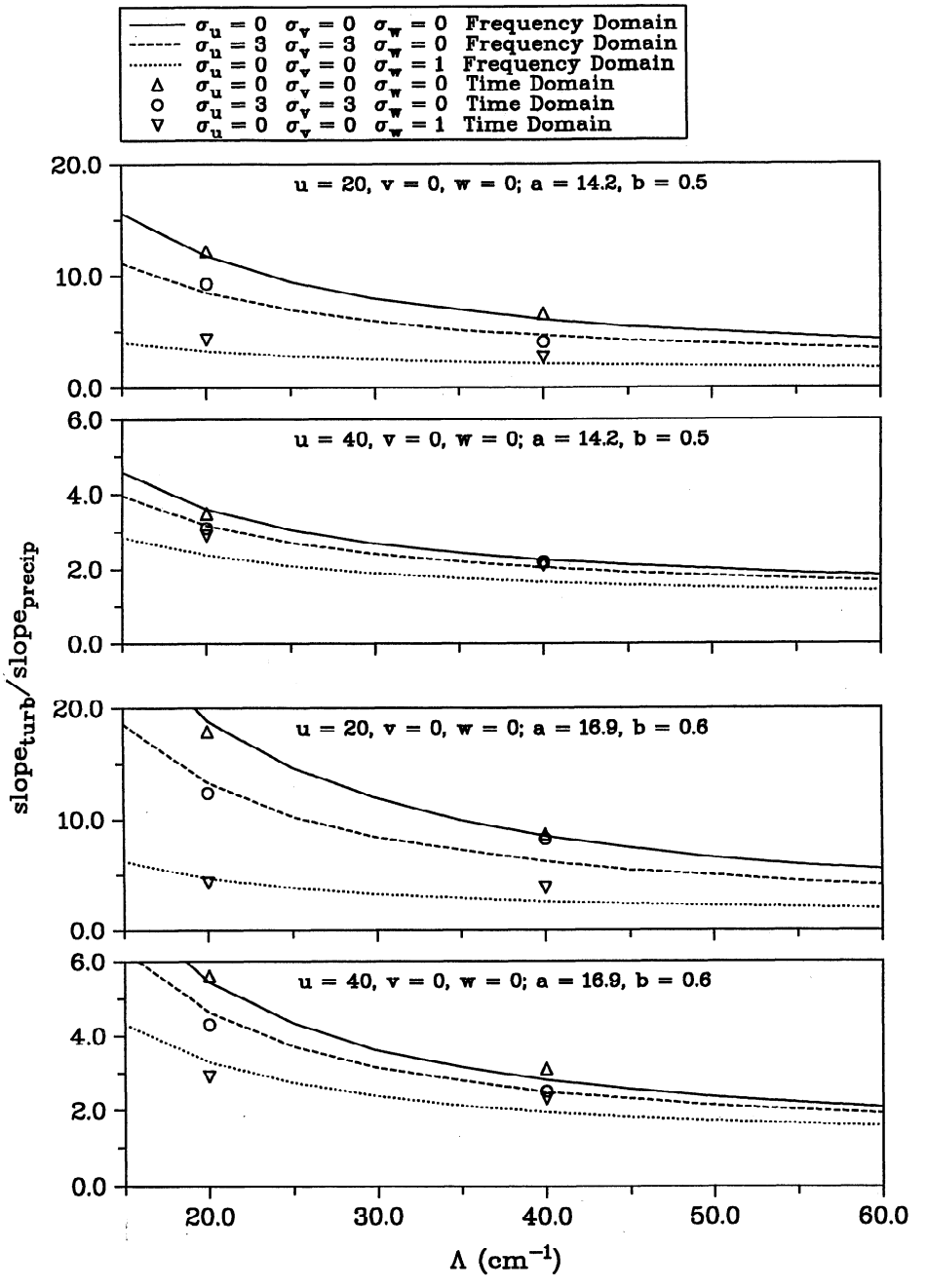

Figure 7. The ratio of the slopes in the cross-spectral phase corresponding to turbulence and precipitation plotted versus Λ. The values u, v, w, σ_u, σ_v, and σ_w are all given in m s^{-1}. The units of a are in m s^{-1} cm^{-b}, and b is unitless.

using cross-spectral data corresponding to precipitation as opposed to turbulent variations in the refractive index. Figure 7 suggests that large errors are to be expected in SI estimates of the apparent horizontal wind for the case when the wind vector is aligned with the antenna baseline. This is especially true if the wind is slight or the air is relatively calm. Although not shown,

similar results to those shown in Figure 7 are also found when the wind vector is not parallel to the antenna baseline. Naturally if a cross spectrum contains peaks from both precipitation and turbulence then one would choose the latter when making wind estimates. If, however, the backscattered signal from the precipitation is dominant, then only one peak will be available. This consideration becomes increasingly relevant with the advent of radar interferometers operating at 915 and 1290 MHz, which are more sensitive to Rayleigh scatter from precipitation.

In addition to illustrating the enhanced overestimation of the apparent horizontal wind when using cross-spectral data from precipitation, Figure 7 also indicates that SI observations may be used to extract information about the drop size distribution. If the cross-spectral data are available containing both a turbulent peak and a precipitation peak, then the slopes of the phase could be used, for example, to estimate Λ or μ as given in (4). As seen in Figure 7, a particular ratio of slopes does not uniquely represent a given set of atmospheric parameters. However, given estimates of u, v, and w along with their variances, an iterative least squares calculation in the frequency domain might yield the parameters pertaining to the precipitation.

The results from the time domain and the frequency domain simulations presented in Figure 7 show reasonably good agreement; however, there are discrepancies. Denoting the ratio of the slopes by $\gamma = \text{slope}_{\text{turb}} / \text{slope}_{\text{precip}}$, the average deviation between the values plotted in Figure 7 given by $1/\text{N} \sum_1^N (\gamma_{\text{freq}} - \gamma_{\text{freq}})/\gamma_{\text{freq}}$ is 0.128. The subscripts indicate whether the ratio was found using the time domain or the frequency domain simulation. As was mentioned earlier, the time domain spectra were calculated using only five coherent integrations, and the fluctuations seen in the linear portions of the cross-spectral phase create uncertainties when estimating the slope. These uncertainties probably contribute to the majority of the deviations between the two methods. Further analysis involving radar observations, calculations of the drop size distributions, and predictions using the two simulations are needed to resolve the utility of such a method for estimating Λ or μ.

7. Conclusions

This paper has focused on the effects of precipitation on spatial radar interferometry. Spatial interferometry has been shown to be a useful tool in studying many phenomena associated with the lower and middle atmosphere. Recently SI has also been applied in an investigation of precipitation. Precipitation data were collected at the MU radar in Japan while operating in a mode that facilitated an SI analysis of the observations. Fortunately, during the time of the observations, backscattered signals from the hydrometeors and the turbulent variations of the refractive index were in the correct proportions to provide bimodal spectra in certain range gates. In those cases a linear trend in the cross-spectral phase can be identified for each contribution provided the Doppler spectra are sufficiently well separated in velocity.

As a first approximation, we can consider the precipitation particles to be advected with the air motions. The slopes in the cross-spectral phase associated with the turbulence and the rain should then be the same. The data from the MU radar observations, however, show this not to be the case, and more specifically, the slopes from the precipitation contribution are systematically less than those from the turbulence. It is known that a fading mechanism resulting from turbulence will bias the cross-spectral phase toward zero. The cross-spectral data from the precipitation should likewise be influenced by turbulent fading. This does not, however, account for the enhanced reduction of the slope. It has been proposed that the further decorrelation results from the distribution of the precipitation particles contained within the radar sampling volume. The spectral peak attributed to the precipitation is broadened in velocity space through the spread of the Doppler fall speeds. Any temporal decorrelation resulting from such velocity

spreading should lead to an underestimation of the slope.

To test the supposition that a DSD might contribute to precipitation fading, two simulations have been presented. The simulations are meant to approximately model the atmospheric conditions present during the time of the MU radar observations. Not only did the simulations show a fading mechanism resulting from the distribution of the precipitation fall speeds, but it was found that the degree of fading is dependent on the parameters of the DSD. Furthermore, the speed with which calculations can be made in the frequency domain provide hope for extracting drop size information from observed Doppler spectra using SI. By comparing the slope in the cross-spectral phase associated with the air motion peak and the precipitation motion peak, the frequency domain simulation may provide a means of deducing Λ or possibly μ in (4). Although the degree by which the cross-spectral phase is biased depends on several parameters, namely the air motions, the parameters of the precipitation fall speed law, and the shape of the DSD, calculations could be conducted in the frequency domain through an iterative process. This would be too time consuming in the time domain.

This study has not addressed several points that should be considered in future investigations. Work is needed to establish the potential role of SI in the study of precipitation. We have seen that the presence of precipitation can bias SI estimates of the horizontal wind, but how can we correct for this effect? FCA or FSA methods have been invoked in the past to correct for turbulent fading in clear-air scatter. These methods, however, assume Gaussian correlation functions. Although this should not be the case for scatter from precipitation, it might prove to be a sufficient approximation, especially when turbulence is present. Even if the precipitation fading is not corrected, we should establish some statistical criteria to determine how much the presence of precipitation will bias SI wind estimates for a particular radar frequency. This is particularly important considering that interferometry is currently being implemented at the higher frequencies of 915 and 1290 MHz. Another feature of SI that has not been exploited in this study is its ability to locate scatterers within the sampling beam. Conventional Doppler radars average the contributions from all scatterers within the pulse volume. Consequently, some of the more localized features associated with precipitation, such as rain shafts and channels from lighting discharges become partially lost in the background signal. The phase information available in SI measurements could be used to isolate such features.

Acknowledgments. We would like to thank Lamar Sheppard for his help in implementing the time domain computer model. P. B. C. and C. W. U. were supported by the NSF under grant ATM9003448, and R. D. P. under NSF grants ATM9311989 and ATM9301108. M. F. L. was supported by AFOSR grant AFOSR-91-0384. The MU radar belongs to and is operated by the Radio Atmospheric Center of Kyoto University, Japan.

References

Atlas, D., and C. W. Ulbrich, Path- and area-integrated rainfall measurements by microwave attenuation in the 1–3 cm band, *J. Appl. Meteorol.*, *16*, 1322–1331, 1977.

Atlas, D., R. C. Srivastava, and R. S. Sekhon, Doppler radar characteristics of precipitation at vertical incidence, *Rev. Geophys.*, *11*, 1-35, 1973.

Briggs, B. H., The analysis of spaced sensor records by correlation techniques, in *Handbook for MAP*, vol. 13, pp. 166–186, SCOSTEP Secretariat, University of Illinois, Urbana, 1984.

Briggs, B. H., and R. A. Vincent, Spaced-antenna analysis in the frequency domain, *Radio Sci.*, *27*, 117–129, 1992.

Chilson, P. B., R. D. Palmer, M. F. Larsen, C. W. Ulbrich, S. Fukao, M. Yamamoto, T. Tsuda, and S. Kato, First observations of precipitation with a spatial interferometry, *Geophys. Res. Lett.*, *19*, 2409–2412, 1992.

Chu, Y.-H., L.-P. Chian, and C.-H. Liu, The investigation of the atmospheric precipitations

by using Chung-Li VHF radar, *Radio Sci.*, *26*, 717–729, 1991.

Doviak, R. J., and D. S. Zrnić, *Doppler Radar and Weather Observations*, 458 pp., Academic, San Diego, Calif., 1984.

Farley, D. T., H. M. Ierkic, and B. G. Fejer, Radar interferometry: A new technique for studying plasma turbulence in the ionosphere, *J. Geophys. Res.*, *86*, 1467–1472, 1981.

Larsen, M. F., and J. Röttger, The spaced antenna technique for radar wind profiling, *J. Atmos. Oceanic Techol.*, *6*, 920–938, 1989.

Larsen, M. F., R. D. Palmer, S. Fukao, R. F. Woodman, M. Yamamoto, T. Tsuda, and S. Kato, An analysis technique for deriving vector winds and in-beam incidence angles from radar interferometer measurements, *J. Atmos. Oceanic Technol.*, *9*, 3–14, 1992.

Marshall, J. S., and W. M. Palmer, The distribution of raindrops with size, *J. Meteorol.*, *5*, 165–166, 1948.

Meek, C. E., An efficient method for analyzing ionospheric drifts data, *J. Atmos. Terr. Phys.*, *42*, 835–839, 1980.

Palmer, R. D., M. F. Larsen, R. F. Woodman, S. Fukao, M. Yamamoto, T. Tsuda, and S. Kato, VHF radar interferometry measurements of vertical velocity and the effect of tilted refractivity surfaces on standard Doppler measurements, *Radio Sci.*, *26*, 417–427, 1991.

Papoulis A., *Probability, Random Variables, and Stochastic Processes,* 3rd ed., 666 pp., McGraw-Hill, New York, 1991.

Röttger, J., and R. A. Vincent, VHF radar studies of velocities and irregularities using spaced antenna techniques, *Geophys. Res. Lett.*, *5*, 917–920, 1978.

Röttger, J., C. H. Liu, J. K. Chao, A. J. Chen, C. J. Pan, and I. J. Fu, Spatial interferometry measurements with the Chung-Li VHF radar, *Radio Sci.*, *25*, 503–515, 1990.

Sekhon, R. S., and R. C. Srivastava, Doppler radar observations of drop-size distributions in a thunderstorm, *J. Atmos. Sci.*, *28*, 983–994, 1971.

Sheppard, E. L., and M. F. Larsen, Analysis of model simulations of spaced antenna/radar interferometer measurements, *Radio Sci.*, *27*, 759–768, 1992.

Sheppard, E. L., M. F. Larsen, R. D. Palmer, S. Fukao, M. Yamamoto, T. Tsuda, and S. Kato, A statistical comparison of spaced antenna and spatial interferometry wind estimation, *Radio Sci.*, *28*, 585–593, 1993.

Sidi, C., and J. Barat, Observational evidence of an inertial wind structure in the stratosphere, *J. Geophys. Res.*, *91*, 1209–1217, 1986.

Spilhaus, A., Raindrop size, shape, falling speed, *J. Meteorol.*, *5*, 108–110, 1948.

Tsuda, T., T. Sato, K. Hirose, S. Fukao, and S. Kato, MU radar observations of the aspect sensitivity of backscattered VHF echo power in the troposphere and lower stratosphere, *Radio Sci.*, *21*, 971–980, 1986.

Ulbrich, C. W., Natural variations in the analytical form of the raindrop size distribution, *J. Clim. Appl. Meteorol.*, *22*, 1764–1775, 1983.

Van Baelen, J. S., and A. D. Richmond, Radar interferometry technique: Three-dimensional wind measurement theory, *Radio Sci.*, *26*, 1209–1218, 1991.

Van Baelen, J. S., T. Tsuda, A. D. Richmond, S. K. Avery, S. Kato, S. Fukao, and M. Yamamoto, Comparison of VHF Doppler beam swinging and spaced antenna observations with the MU radar: First results, *Radio Sci.*, *25*, 629–640, 1990.

Van Baelen, J. S., A. D. Richmond, T. Tsuda, S. K. Avery, S. Kato, S. Fukao, and M. Yamamoto, Radar interferometry technique and anisotopy of the echo power distribution: First results, *Radio Sci.*, *26*, 1315–1326, 1991.

Vincent, R. A., and J. Röttger, Spaced antenna VHF radar observations of tropospheric velocities and irregularities, *Radio Sci.*, *15*, 319–335, 1980.

Vincent, R. A., P. T. May, W. K. Hocking, W. G. Elford, B. H. Candy, and B. H. Briggs, First results with the Adelaide VHF radar: Spaced antenna studies of tropospheric winds, *J. Atmos. Terr. Phys.*, *49*, 353–366, 1987.

Woodman, R. F., Inclination of the geomagnetic field measured by an incoherent scatter technique, *J. Geophys. Res.*, *76*, 178–184, 1971.

Woodman, R. F., and A. Guillén, Radar observations of winds and turbulence in the stratosphere and mesosphere, *J. Atmos. Sci.*, *31*, 493–505, 1974.

P. B. Chilson, Max - Planck - Institut für Aeronomie, Postfach 20, D-37189 Katlenburg-Lindau, Germany. (e-mail: chilson@linax1.mpae.gwdg.de)

S. Fukao, M. Yamamoto, T. Nakamura, and S. Kato, Radio Atmospheric Science Center, Kyoto University, Kyoto 611, Japan. (e-mail: fukao@kurasc.kyoto-u.ac.jp; yamamoto@kurasc.kyoto-u.ac.jp; kato@kurasc.kyoto-u.ac.jp)

M. F. Larsen, and C. W. Ulbrich, Department of Physics and Astronomy, Clemson University, Clemson, SC 29634-1911. (e-mail: mlarsen@hubcap.clemson.edu; cwu@clouds.phys.clemson.edu)

R. D. Palmer, Department of Electrical Engineering and Center for Electro-Optics, University of Nebraska, 209 N. Walter Scott Eng. Ctr., Lincoln, NE 68588-0511. (e-mail: bpalmer@unlinfo.unl.edu)

(Received April 2, 1994;
accepted September 19, 1994.)